

Case Report

# Flood Response System—A Case Study

Yogesh Kumar Singh <sup>1,\*</sup>, Upasana Dutta <sup>1</sup>, T. S. Murugesh Prabhu <sup>1</sup>, I. Prabu <sup>1</sup>, Jitendra Mhatre <sup>1</sup>, Manoj Khare <sup>1</sup>, Sandeep Srivastava <sup>1</sup> and Subashisa Dutta <sup>2</sup>

<sup>1</sup> Emerging Solutions & e-Governance Group, Center for Development of Advanced Computing (C-DAC), Pune 411008, India; upasanad@cdac.in (U.D.); murugeshp@cdac.in (T.S.M.P.); iprabu@cdac.in (I.P.); jitendram@cdac.in (J.M.); manojk@cdac.in (M.K.); sandeepk@cdac.in (S.S.)

<sup>2</sup> Civil Engineering Department, Indian Institute of Technology, Guwahati 781039, India; subashisa@iitg.ernet.in

\* Correspondence: yogesh.cdac@gmail.com or yogesh@cdac.in; Tel.: +91-20-25503250

Academic Editors: Angelica Tarpanelli, Luca Brocca and Mauro Rossi

Received: 22 February 2017; Accepted: 26 May 2017; Published: 7 June 2017

**Abstract:** Flood Response System (FRS) is a network-enabled solution developed using open-source software. The system has query based flood damage assessment modules with outputs in the form of spatial maps and statistical databases. FRS effectively facilitates the management of post-disaster activities caused due to flood, like displaying spatial maps of area affected, inundated roads, etc., and maintains a steady flow of information at all levels with different access rights depending upon the criticality of the information. It is designed to facilitate users in managing information related to flooding during critical flood seasons and analyzing the extent of damage. The inputs to FRS are provided using two components: (1) a semi-automated application developed indigenously, to delineate inundated areas for Near-Real Time Flood Monitoring using Active Microwave Remote Sensing data and (2) a two-dimensional (2D) hydrodynamic river model generated outputs for water depth and velocity in flooded areas for an embankment breach scenario. The 2D Hydrodynamic model, CCHE2D (Center for Computational Hydroscience and Engineering Two-Dimensional model), was used to simulate an area of 600 km<sup>2</sup> in the flood-prone zone of the Brahmaputra basin. The resultant inundated area from the model was found to be 85% accurate when validated with post-flood optical satellite data.

**Keywords:** Flood Response System; Microwave analysis; Flood inundation mapping; Damage assessment; GIS based decision support system

## 1. Introduction

Floods are one of the most, widespread, frequent, and recurring natural disasters. About 2641 flood disasters across the globe were recorded in the Dartmouth Flood Observatory catalogue [1] between 2000 and 2007, affecting 2051 different rivers. A study shows that floods consume up to one-third of humanitarian aid [2], causing \$20 billion annually in damages and affecting up to 100 million people annually [3]. A recent report by the United Nations, “The Human Cost of Weather Related Disasters,” reveals that in the last 20 years, 157,000 people have died globally as a result of floods. The report also says that between 1995 and 2015 floods affected 2.3 billion people [4], which accounts for as many as 56% of all those affected by weather-related disasters [5]. This data makes flooding, undoubtedly, the most destructive phenomenon across the world. Floods are a consequence of the increasing frequency of heavy rains, changes in upstream land-use, and a continuously increasing concentration of population and assets in the flood plains [6]. Floods can occur anywhere as a result of heavy rain and can be of different intensities—from small flash floods to sheets of water engulfing huge areas of land, causing destruction either way.

Like most parts of the world, India is vulnerable to floods taking a toll on its economic, social, and human resource potential and affecting growth, development, productivity, and macroeconomic performance in the long run. According to the National Flood Commission of India (1980), the annual average of land area and crop area affected by flooding is about 1.86 and 0.037 million km<sup>2</sup>, respectively, which is about 0.4 million km<sup>2</sup> out of a total geographical area of 3.29 million km<sup>2</sup>. The average loss in financial terms is about INR 13,000 million [7].

Both at the global and national scale, water authorities face various functional challenges when monitoring floods using their river networks. First, the cost of maintaining gauging stations can be a limiting factor, particularly in a large country like India. This renders the gauging stations out of service or inaccessible, hence creating gaps in the hydrograph time series. Secondly, there are many rivers that go through national boundaries and, due to political and administrative reasons, information and data on the river in upstream countries are not always communicated to the downstream countries. This creates serious lapses in data and hampers effective flood prediction. Thirdly, there are no physical tools to measure the extent of the flooding. Obtaining information on the extent of flooding is a challenge for emergency managers, requiring aerial reconnaissance or satellite imagery [8].

Over the years, advances have been seen in remote sensing measurements, which are gradually replacing or compensating in situ measurements. Aerial reconnaissance has been effective for determining the spatial extent of coastal and river flooding in detail for relatively small areas [9–12]. River discharge estimates can also be obtained using high-resolution satellite data and a few ground measurements [13,14].

Even though the use of image data from optical satellite sensors (like Pan, LISS, etc.) in the visible or infrared portion of the spectrum is very useful for studying land features, their usefulness is limited during the monsoon season due to cloud cover being visible on the image. On the other hand, the microwave portion of the spectrum gives cloudless images even during the monsoon season [15]. Microwave remote sensing data can penetrate clouds, emergent aquatic plants, and forest canopies to detect water [16–18]. Cloud penetration is particularly important for monitoring flood events because they commonly occur during hurricane-related flooding or periods of extended rainfall [18–20]. However, for most remote sensing solutions, the revisit frequency (i.e., the time between two measurements in the same place) is too low for monitoring purposes, or the spatial coverage is limited [20]. Both active [21] and passive data [22] have been extensively explored by the authors for extracting flood monitoring with different level of details as per resolution of the data used.

Floods are natural hazards and cannot be prevented; with improper land use and negligible land cover management, areas are becoming more vulnerable and, as a result, floods are becoming more disastrous [23]. Many measures are being taken to make floods more manageable. Some engineering techniques such as marginal embankments or dykes have been adopted to control the flood inundation of the flood plain area up to a certain extent in India. However, the higher the embankment height, the higher is the associated risk of breaching. Extensive flooding can be the result of levee system failures, most frequently caused by the piping process due to seepage [24,25]. In addition, changing river morphology also makes the embankment more vulnerable, which can frequently be seen in a highly braided river like the Brahmaputra. It is necessary to study beforehand the associated risks, once the embankment breaches [26]. This type of study requires accurate flood plain topography data, which is very difficult to obtain in the case of developing countries like India. Utilizing the developments in mathematical river models, the flood inundation phenomenon can be modeled using the available floodplain topography with reasonable accuracy [27]. Several investigators have used 1D and 2D river models to simulate the flood inundation phenomenon.

In this study, a Flood Response System (FRS) was developed to monitor flooding in near real time using active Microwave Remote Sensing data. A 2D hydrodynamic river model (CCHE2D) was used to simulate the embankment breach scenario. CCHE stands for “Center for Computational Hydro-science and Engineering” developed by the National Center for Computational Hydro-science and Engineering, University of Mississippi, USA [28].

FRS was developed as an easy-to-use and robust decision-making tool to collate flood and socio-economic information. Timely information helps with timely mitigation and eventually effective rescue operations. FRS kept this as the prime focus and offered a solution for effectively monitoring & reporting flood-like disasters in a short span of time. Due to a lack of linkage between policy-making, socioeconomic benefits, and flood disasters, lots of valuable data and information are gathered/generated but do not reach the right person at the right time. FRS pays special attention to this aspect both for generation of data in near real time and dissemination of the same to people in the fastest possible manner so that the purpose of the work does not get defeated.

## 2. Background & Objective

Brahmaputra valley and flooding are almost synonymous. Every year thousands of acres of land remain underwater for most of the year in this valley. One of the important causes of frequent flooding in this region is the dynamic monsoon rainfall regime against the backdrop of the unique physiographic setting. Also, the water yield of the Brahmaputra valley is among the highest in the world. This, together with the high sediment yield, limited width of the valley, and abruptly flattened gradient, leads to tremendous drainage congestion and resultant flooding. The scenario is further exacerbated by a myriad of social, economic, and environmental factors causing increased vulnerability of people to flooding [29].

Timely information about flooding provides strong indicators of a forthcoming disaster. However, owing to the unpredictability of the behavior of the Brahmaputra River and the increased incidence of anthropogenic activities on it, real-time estimations of the aftermath will help to reduce, manage, and control the extent of the disaster. Also, a major pool of both finance and research is being channeled towards forecasting floods in this valley but with little or no improvement in actually monitoring and managing floods and their repercussions. This calls for a different approach to handling such natural disasters. Hence, real-time monitoring and analysis of such a recurring hazard is essential.

In Austin, Texas, some authors proposed that communities, led by emergency management officials, work with federal, state, and local entities to create a Community Flood Response System, based on three components: a flood response map book, a personal flood response guide, and a web-based flood emergency information system that exists within the community's Emergency Operations Center [30].

In India, a two-tier system of flood management exists: a state level mechanism and a central government mechanism. The State Government Mechanism includes the Water Resources Departments, Revenue Department, State Technical Advisory Committee, and Flood Control Board. In some States, the Irrigation Departments and Public Works Departments are responsible for matters related to flood management. The Central Government Mechanism includes the Union Government, which has set up dedicated organizations and various expert water and flood committees to enable the state governments in addressing flooding problems in a comprehensive manner [31]. However, even after a well-placed mechanism, certain lacunae were observed in the process of data and information acquisition during the floods in the study area concerned. The process was mostly manual in nature, wherein information sometimes less or over-projected, was communicated verbally from the village level to the district level. The district administration and the state administration also received satellite-based information of inundation but sometimes the information is received as much as a week later. Also, the inundation information is received as maps, which are of less importance during active Rescue and Relief (R & R) operations. It was more of a visual aid than operational. Armed with the district flood contingency plans and the information received from ground zero, current flood plans are laid for the R & R operations. This is the traditionally used method, which has many factual and operational errors. Due to a lack of any scientific verification system, most of the time R & R operations do not reach the affected regions on time.

To strengthen this traditional approach, FRS was designed. FRS is a network-enabled, GIS-based solution developed using open-source software and libraries. It has flood damage assessment

query-based modules with outputs in the form of spatial data, a statistical database, and theme-based maps. FRS effectively facilitates the management of various activities related to disasters caused due to flood and maintains a steady flow of information at all levels. It is designed to facilitate users in managing information related to flooding during critical seasons and analyzing the extent of damage in near real time.

FRS was aided by microwave remote sensing to help plan and execute efficient emergency response and post disaster management measures. FRS uses microwave data to utilize its cloud penetration, all-weather, and day-and-night data acquisition capability. This helps in generating effective information on the status of land use in drainage basins during the monsoon season. Mathematical transformation and thresholding-based microwave data analysis were used for automatic extraction of the inundated areas. This helps in gathering near real-time information in a holistic manner. This information was translated into parameters and coefficients as input for the hydrological models used for runoff and flood forecasting. FRS uses this microwave data along with other ancillary information to derive flood response information for the end user to operate in near real time. It also has a probabilistic flood information module to predict inundation due to breaches in the embankment made along the Brahmaputra and Subansiri for a given flood hydrograph.

### 3. Study Area and Regional Hydrology of the Area

#### 3.1. North Lakhimpur, Assam

Located in the northeast corner of the Indian state of Assam, the district of Lakhimpur lies on north bank of the Brahmaputra (Figure 1). It is bounded on the north by the Lower Subansiri and Papumpare districts of the state of Arunachal Pradesh and on the east by Dhemaji district. Majuli, the largest river island belonging to Jorhat district, is on the south and Gohpur subdivision of Sonitpur district is on the west.

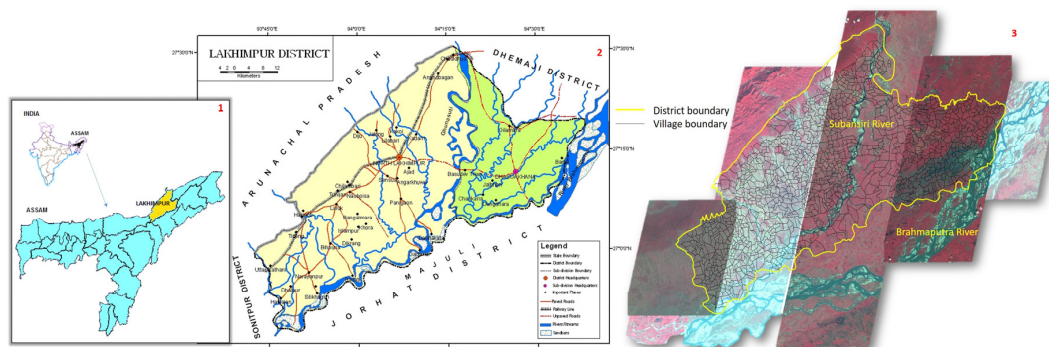


**Figure 1.** (1) Map of India and Assam state; (2) administrative map of Lakhimpur district; (3) mosaic of LISS imageries of study area. Total study area: 2277 km<sup>2</sup>, out of which 2257 km<sup>2</sup> is rural and 20 km<sup>2</sup> is urban.

Lakhimpur district is one of the most flood-ravaged districts of Assam. Flooding in the district is the result of cumulative incidences. It can be attributed to excessive rainfall in Assam and Arunachal Pradesh, snow melt in Tibet, and the bursting of natural dams formed by landslides on the rivers flowing from Arunachal Pradesh. During flooding the river gets charged with an enormous quantity of silt. Movement of this silt in the river alters the flow conditions and sometimes changes the river's course, causing havoc in its downstream basin.

#### 3.2. The River System

**The Brahmaputra:** Undoubtedly the most dynamic and awe-inspiring river of India, Brahmaputra has a few unique characteristics. It is fed by numerous tributaries, rivulets, and streams.

Added to all these are the wide and divergent braids of the Brahmaputra and the meanders that issue from it, resulting in an intricate maze of water bodies spread not merely across the valley, but also enclosing it. The Brahmaputra is fed on its course through the valley by no fewer than 57 tributaries on its north bank and 33 on its south bank.

Out of northeast India's total regional area of 0.225 million km<sup>2</sup>, the Brahmaputra drainage system covers 0.175 million km<sup>2</sup>. Most of its area receives an average annual rainfall of nearly 200 cm. The maximum discharge of the river at Dhubri (where it enters Bangladesh) is 0.0019822 million cumecs.

**The Subansiri:** The Subansiri is the largest tributary of the Brahmaputra. It originates in the south of Po Rom peak (5059 m) and enters Assam through Arunachal Pradesh. Its total length is 520 km and it drains a basin of 37,000 km<sup>2</sup>. The river maintains an almost stable course but becomes unstable as soon as it enters the alluvial plains of Assam in North Lakhimpur.

The mean daily discharge of Subansiri at Gerukamukh is 138,842 cumecs. The average annual sediment yield at Chauldhuaghat is  $94.83 \times 10^3$  tons. The river discharges 5938 cumecs of water at Bhimpara Ghat. The Subansiri at maximum discharge brings down boulder gravel, sand, and debris during flood [32].

#### 4. Data

A range of remote sensing satellite data (both optical and microwave), spatial and non-spatial data were used in the study. The projection parameters were defined keeping in mind the minimum data loss and distortions. Parameters were kept consistent according to the parameters used by the National Remote Sensing Centre (NRSC) so that in future easy integration with other projects or data is possible. Some of the data used have been elucidated below.

##### 4.1. Microwave Remote Sensing Data

Different sets of microwave (MW) remote sensing data were used in the study. Data types and dates for the MW were decided according to the temporal and spatial resolution and the flood cycle prevalent in the study area. Data type selection depended on the polarization of return and incident beam suitable for proper flood identification. Availability of the data during the particular time period required proved to be a critical issue. RADARSAT 1 data was finally selected due to its distinct advantages over its counterparts.

RADARSAT-1 Synthetic Aperture Radar (SAR) Imagery taken on four separate dates were used. Two of them were Standard 7 beam mode and one was SAR Wide 2.

- 28 June 2002—Pre-flood image (Standard 7 beam mode, S7)
- 17 July 2003—During-flood image (Standard 7 beam mode, S7)
- 14 June 2002—Pre-flood image (SAR Wide 2 beam mode, W2)
- 23 June 2008—Pre-flood image (ScanSAR Wide beam mode, SWB)

RADARSAT-2 SAR Imagery taken on two separate dates were also used. One of them was ScanSAR Narrow beam mode (polarization: HH + V) and the other is SAR Wide 2 (polarization: HV).

- 6 July 2009—During-flood image (ScanSAR Narrow beam mode, HH + V polarization, SCNB)
- 13 July 2009—During-flood image (SAR Wide 2 beam mode, HV polarization, W2)

##### 4.2. Optical Remote Sensing Data

Optical remote sensing data were used mainly for the validation of inundated area results, obtained from the probabilistic flood information model. Panchromatic imagery of an Enhanced Thematic Mapper (ETM) sensor (March 2007, 10 m spatial resolution) and multispectral imagery of ETM sensor (September 2008, 30 m spatial resolution) were used. Apart from this Linear Imaging Self-Scanning (LISS), IV multi-spectral data of Indian Remote Sensing (IRS) P6 ResourceSat were also used to map and update road networks and land use/land cover in the study area.

#### 4.3. DEM Data

Digital Elevation Model (DEM) data from *Shuttle Radar Topography Mission* (SRTM) (90 m spatial resolution) was used for the probabilistic flood information model.

#### 4.4. Derived/Model Input Data

The following data were used for the 2D flood inundation modeling:

- Channel geometry (cross-section, bed slope)
- Channel roughness (Manning's coefficient)
- Discharge (daily discharge data)
- Flood plain characteristics (land use/land cover and its extent)

#### 4.5. Ancillary Data

Ancillary data included Survey of India Toposheets, Data from Line departments, Deputy Commissioner's (DC) Office, New Lakhimpur (NLP) & State Disaster Management Authority, and meteorological data from the Indian Meteorological department. For infrastructure and population information, census data (2001) was collected from the Census of India.

### 5. Methodology & Process

The project was divided into four major components: spatial & non-spatial data preparation, microwave data analysis to obtain inundated area, hydrodynamic simulation for an embankment breach scenario, and software development/web interface for information dissemination.

#### 5.1. Spatial & Non-Spatial Data

A few spatial layers were created (some derived and some extracted using imageries and ancillary information) using standard GIS procedures, including scanning of hardcopy maps followed by conversion into digital GIS format with the help of ESRI<sup>R</sup> ArcGIS<sup>TM</sup> software (Esri India Technologies Ltd., Noida, India). In particular, the following layers were provided:

- Administrative boundaries (district/block/revenue circle/village)
- Land use/Land cover classes
- Roads network
- Railways network
- River (major and micro) network
- Wetland
- Habitations
- Embankment

The GIS data formats used in the system are:

- Shape (.shp) Files: a popular geospatial vector data format for GIS, which spatially describes geometries like points, polylines, and polygons.
- PostGIS: a spatial database extension for PostgreSQL that "spatially enables" the PostgreSQL server, to be used as a backend spatial database for Geographic Information Systems (GIS).
- A few layers such as the road network and land use/land cover were also updated using IRS P6 LISS IV data and Google maps.

In a highly flood-affected alluvial region, administrative boundaries needed constant updating; some—for instance, the village administrative boundaries—required yearly modification. Most parts

of the virtual administrative boundary wash away and entire villages can vanish or shift to the next district. Hence, special care was taken while preparing these layers.

The non-spatial data included water level data and boat availability. These data were provided by the line departments (Block Development Office) mentioned above. They were further converted from the hardcopy format provided into tabular information.

Boat availability data (a feature unique to the region as every house has a boat to its name) is an important asset during the floods for the R & R operations. This was included as a special request from the DC of the Lakhimpur district with inclusion of additional contact information of the owners.

## 5.2. Microwave Data Analysis

A semi-automatic method of classifying water and other pixels from the microwave/RADAR image was applied in the study. The method involved a user input for threshold value, whereas every other process (filtering, logarithmic transformation, binary raster to vector conversion) was automated [33]. Multi-temporal single-channel single-polarization SAR image was used for the delineation of water bodies. The semi-automated application was developed using Java programming language. The execution time for one run of application was approximately 8 min for one scene of microwave data covering  $200 \times 200$  km to extract inundated areas, making the method useful for near real-time application.

The advantage of the approach used in this application lies in the fact that it is a simple and robust methodology for water feature delineation from SAR images. Step-wise description of the methodology is as follows.

### Step 1. Pre-processing

Image smoothing was performed by an averaging filter of window size  $5 \times 5$  to reduce speckle noise. Though small features were not visible after averaging, for flood mapping the concern is to delineate water features, which are mappable. Hence, the use of complex speckle filters was avoided.

### Step 2. Logarithmic Transformation and Thresholding

The natural logarithm (log to the base 'e') was computed for every pixel of the smoothed SAR image. The histogram of the microwave image usually has two peaks divided by a valley. The pixels corresponding to the first peak represent water (specular reflection) and the pixels (diffuse reflection) corresponding to the other peaks represent features other than water. This transformation enhances the discrimination of land and water features, which is evident from the histograms shown in Figures 2 and 3. Choosing an arbitrary threshold value (say, pixel value = 3000, shown by a red marker), based on visual inspection of the lowest value of the valley in the histogram (Figure 2), yielded poor delineation of water features from the SAR image. After log transformation, the valley of discrimination between the water and land features is more vivid (valley widening) as shown in Figure 3, and hence a threshold value could be comfortably chosen (say, pixel value = 7.8, shown by a red marker). Also, as seen from the log-transformed image histogram in Figure 3, the values have a small range (6.5–11.0) as compared to the input image (117–65535). This method enhances processing speeds.

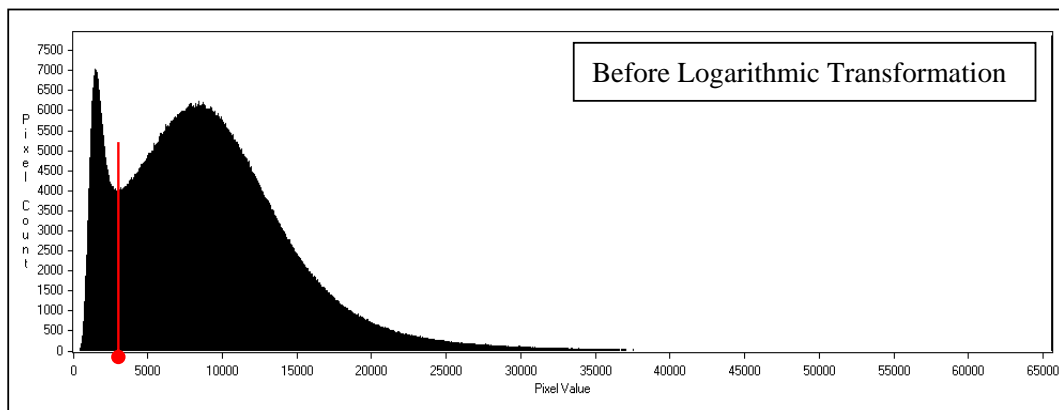


Figure 2. Histogram before logarithmic transformation.

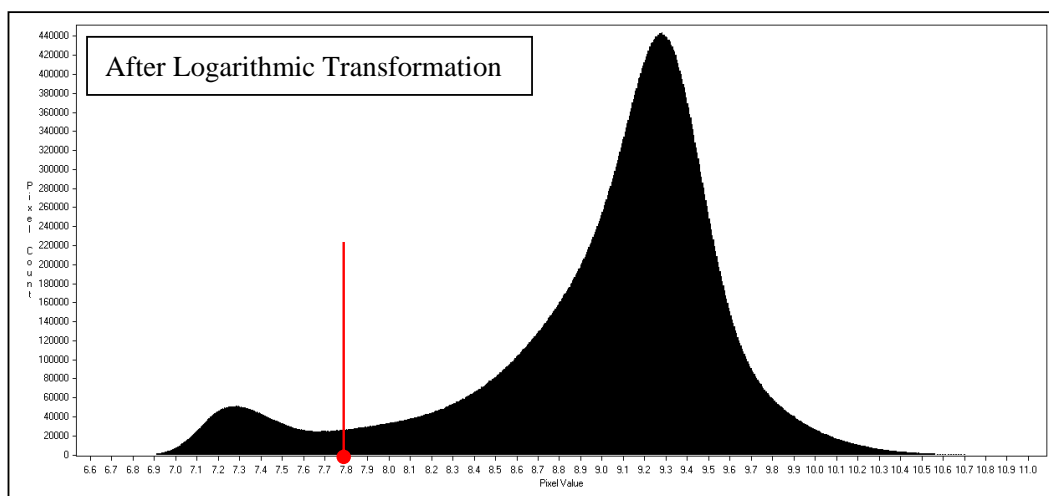
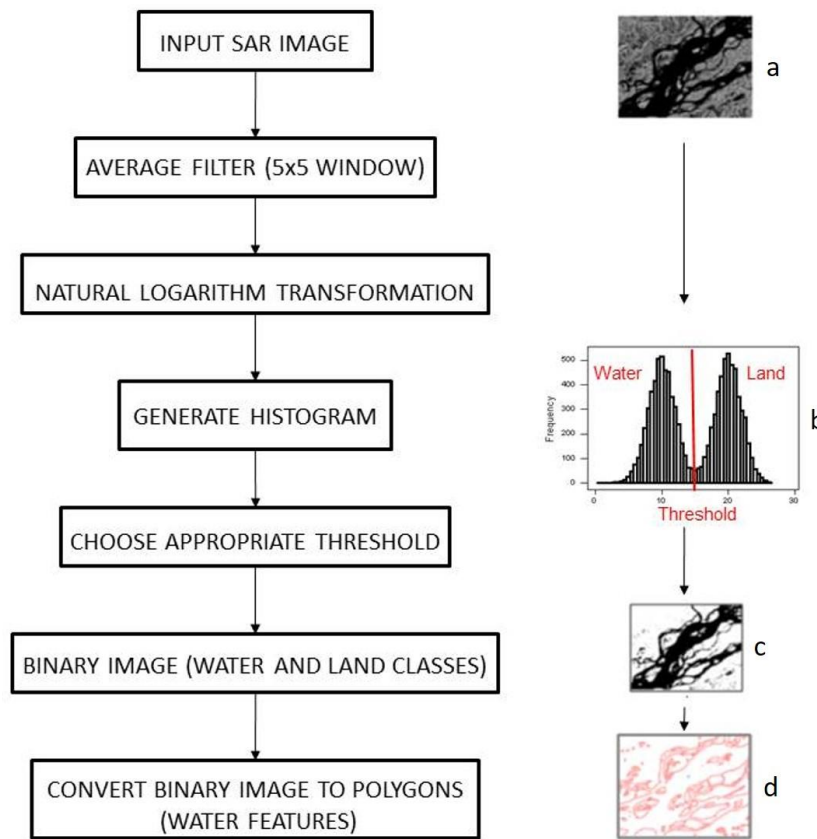


Figure 3. Histogram after logarithmic transformation.

There are two advantages of the logarithmic transformation as depicted in Figures 2 and 3;

- The valley widening in the histogram helps the user to choose the threshold value to classify water and land classes more distinctly.
- The dynamic range of the pixel values that need to be handled by the system after the transformation is very small (65,000 versus 11). This is an essential feature of near real-time systems, as the processing time depends on the dynamic range of the image.

This method works for both the standard SAR and ScanSAR products of RADARSAT-1. This method has the advantage of minimum user input and averts the requirement for a Digital Elevation Model (DEM) and other ancillary data. Hence, this method is simple to implement using open-source libraries and robust enough for operational near real-time flood monitoring applications. The work flow is shown in Figure 4.



**Figure 4.** Workflow for extraction of water features: (a) SAR image, (b) Histogram showing water and land classes, threshold (red line), (c) Binary image (Black is water class), (d) Polygon boundaries of water features.

Creating a flood inundation layer by using GIS is a pre-requisite to generating a flood hazard map, which is a vital component for appropriate land use planning in flood-prone areas. With the help of this system, easily-read, rapidly-accessible charts and maps can be prepared that will facilitate administrators and planners with identifying areas of risk and prioritizing their mitigation/response efforts. This system takes SAR images (raster) as input and delineates water features and generates a flood inundation layer (vector). This layer can be overlaid on village and road layers to visualize the percentage of the area affected by flooding.

This work flow has the following advantages: (a) simple image processing operations; (b) efficient delineation of water features, even at coarser spatial resolutions; (c) less computation time for near real-time application; (d) easy implementation for operational flood mapping purposes; (e) effectiveness at delineating water features efficiently, rapidly, and accurately enough for mapping large areas; and (f) it is a simple algorithm and requires no prior knowledge of the scene and ancillary data such as DEM.

### 5.3. Software Development & Web Interface

The design of the FRS (Figure 5) is based on open-source GIS tools and libraries as well as industry-standard development guidelines. The system was developed using UMN MapServer, ka-Map, PostgreSQL, PostGIS, Apache Web Server, and Windows Server 2003.

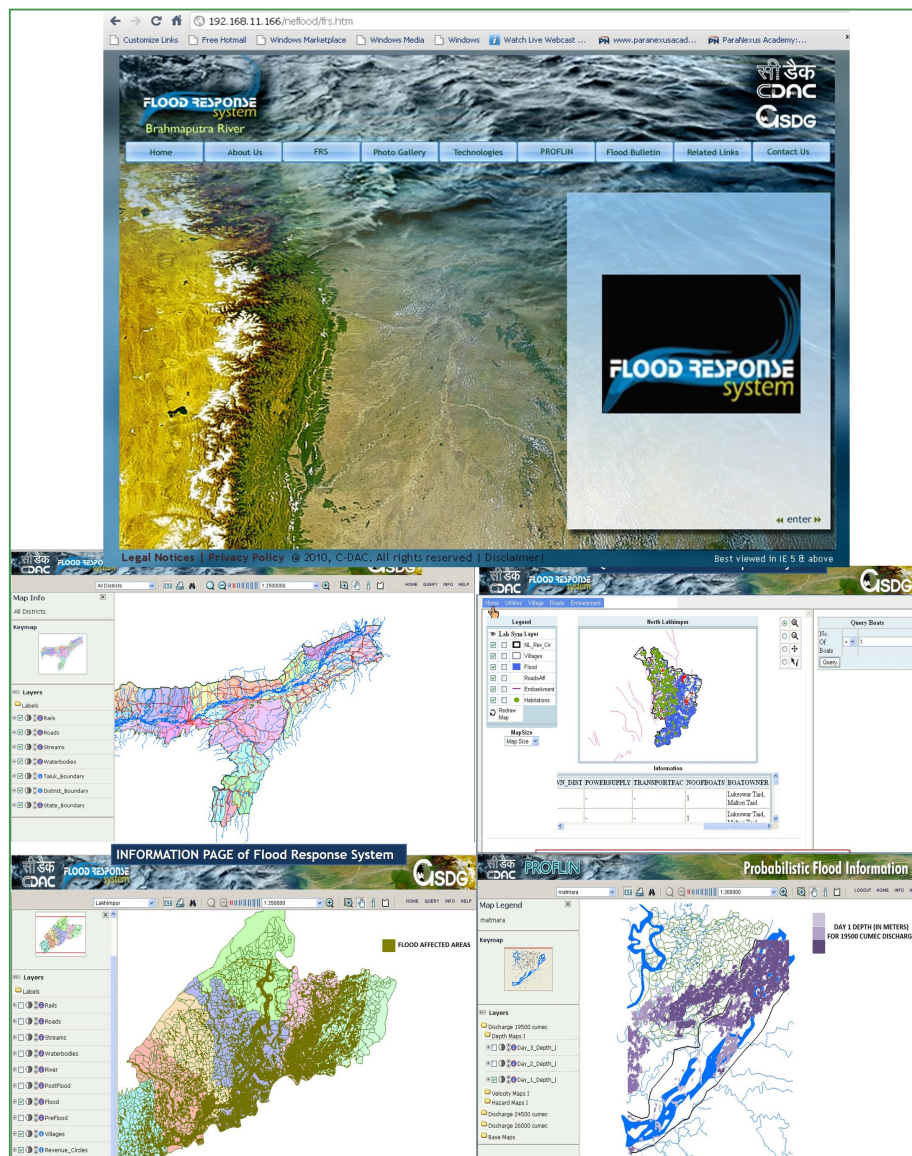


Figure 5. Snapshots of Flood Response System.

### 5.3.1. FRS (Flood Response System)

FRS takes advantage of GIS data/ technologies to plan for flood situations. It uses GIS functionality (like intersection) to find flood-affected areas with the help of different GIS layers. Once the flood-affected areas are identified, information related to those areas like population (census) comes from the relational database, which in turn gives the population affected by flooding and other related queries. FRS is an amalgamation of GIS and Management Information System (MIS) technologies for planning and mitigation of flood response measures. Access to the site was given to users, keeping in mind the transparency and permitted levels of information security (one role for the administrators and one role for other users). English is the primary interface language of the system, although provision for vernacular language is also in the offing.

All of the information available to FRS is accessed through the user interface. The basic interface is entirely tool-driven (Figure 5). It will facilitate users in managing information related to flooding during critical flood seasons and analyzing the extent of damage. The software has been designed for data entry at a single point so as to eliminate repetitive and time-consuming tasks of data compilation and aggregation at various levels. Some of the important modules of FRS are:

- a. The Damage Assessment Module, where general information pertaining to the district's inundated villages and area of inundation can be checked along with information about roads, streams, and rivers.
- b. The Query Module caters to one more level of the administrative unit, wherein the user can get detailed block-level (a block is a smaller unit of a district) information pertaining to floods (e.g., roads, population, nearest schools, etc.) for inundated areas. Layers available for query are—
  - Utilities: boats (owner's information/type of boats), water tanks, medical facilities, nearest schools & colleges, nearest town, transport facilities, electricity availability
  - Village-wide population affected by flooding, percentage area of villages affected
  - Habitations affected
  - Roads affected
  - Embankments affected
- c. The Probabilistic Flood Information Module (PROFLIN) provides information for a probable embankment breach scenario. This is a restricted module of FRS and the information is provided for administrators only. The information present in the system is, at present, for a specific case of Matmara village embankment breach. The module displays on maps the following probable outputs for three consecutive days for various discharge levels (19,500 cumecs, 24,500 cumecs, and 26,000 cumecs) of the river in the floodplains (Figure 6):
  - Velocity maps, in meter per second (for Day 1, Day 2, Day 3)
  - Depth maps, in meters (for Day 1, Day 2, Day 3)
  - Hazard maps (for Day 1, Day 2, Day 3) (based on depth vs. velocity)

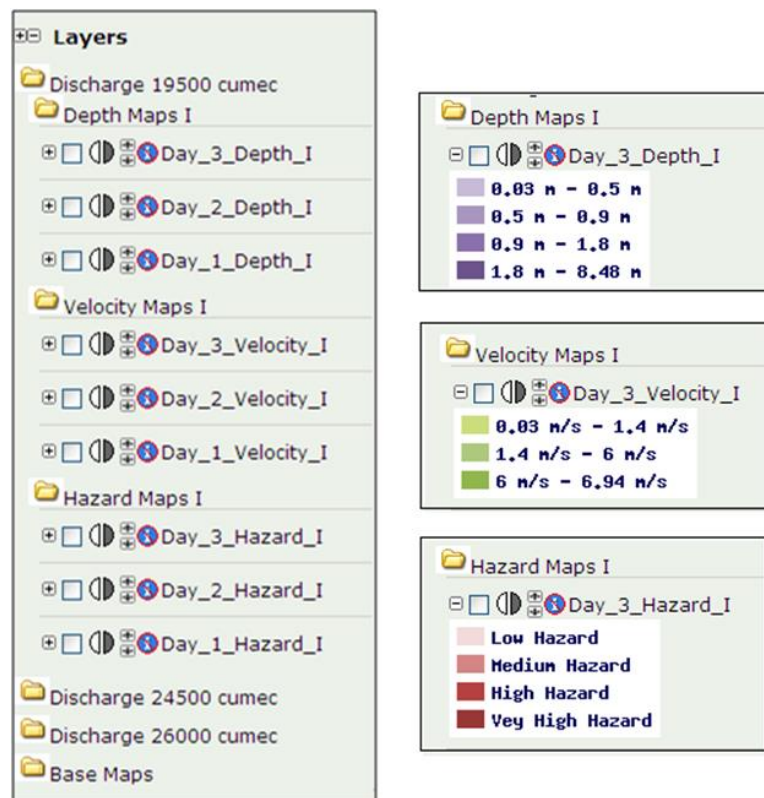


**Figure 6.** Screenshot of layers available in PROFLIN along with legend for depth map, velocity map, and hazard map.

### 5.3.2. Probabilistic Flood Information

Probabilistic flood inundation maps were generated for the study area using the hydroinformatics concept (Figure 7) and the CCHE2D model. Under different inflow hydrograph conditions (for example, a dangerous flood level in the Brahmaputra River and a normal flood level in the Subansiri and other tributaries), flood scenarios were obtained from the simulated results of a mathematical hydrodynamic river model (CCHE2D). A two-dimensional hydrodynamic river model, CCHE2D, which numerically solves depth-integrated Navier–Stokes equations to obtain depth and velocity fields within the chosen domain (river and floodplain), was considered to obtain the spatial variation of the inundation depth and velocity. It can simulate unsteady, turbulent river flow. The simulated results were spatially analyzed to obtain the desired inundation maps, i.e., probable maximum flood inundation depth under different inflow conditions.

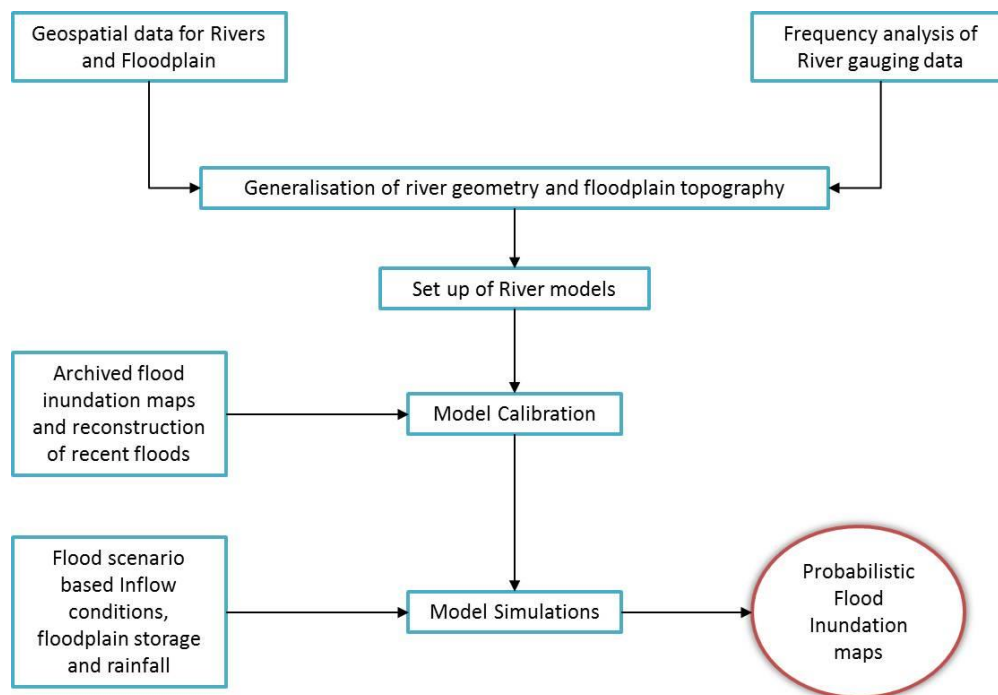


Figure 7. Hydro-informatics-based flood inundation modeling.

Depth-integrated shallow water two-dimensional momentum and continuity equations were solved using CCHE2D model for the study:

$$\frac{\partial w}{\partial t} + \frac{\partial f}{\partial x} + \frac{\partial g}{\partial y} + S = 0 \quad (1)$$

$$\text{With, } w = \begin{bmatrix} H \\ uh \\ vh \end{bmatrix}, f = \begin{bmatrix} uh \\ u^2h + 0.5gh^2 - vh \frac{\partial u}{\partial x} \\ uvh - vh \frac{\partial v}{\partial x} \end{bmatrix}$$

$$S = \begin{bmatrix} 0 \\ gh(I_{Rx} - I_{Sx}) \\ gh(I_{Ry} - I_{Sy}) \end{bmatrix}, g = \begin{bmatrix} vh \\ uvh - vh \frac{\partial u}{\partial y} \\ v^2 + 0.5gh^2 - vh \frac{\partial v}{\partial y} \end{bmatrix},$$

where  $t$  is time,  $g$  is acceleration due to gravity,  $f$  is the Coriolis parameter,  $h$  is the thickness of the fluid layer,  $H = h + z$  is the water surface level above datum level, and  $u$  &  $v$  are the velocity components in the X and Y direction. Sections 4.3 and 4.4 talk about the data required for 2D flood inundation

modeling. The source term  $S$  contains terms for the friction slope  $I_R$  (with its component  $I_{RX}$  and  $I_{RY}$ ) and the bed slope ( $I_{SX}$  and  $I_{SY}$ ). The bed slope in the  $x$  and  $y$  direction is defined by the gradient of bed level  $z$ :

$$I_{SX} = -(\partial z / \partial x) \text{ and } I_{SY} = -(\partial z / \partial y). \quad (2)$$

The model was set up for the flood plain affected by embankment breaching at Matmara village. The study reach was mapped onto a grid with 271 cells in the horizontal and 264 cells in the vertical direction. In the field, this resulted in an average horizontal cell size of  $175 \times 185$  m.

The topography of the floodplain is one of the critical input data types in a flood inundation model. SRTM DEM was used as the topographic data. In order to evaluate the accuracy of this data source, a Differential Global Positioning system (DGPS)-based survey was also conducted. This survey covered a floodplain area in Matmara, an embankment breaching-affected area, North Lakhimpur district, and a north–south survey transect starting from Lakhimpur town to Majuli Island. The length of the transect was about 33 km and its relief was about 10 m. In the floodplain at the embankment breach location, the difference in elevation obtained from the SRTM data and DGPS survey points was found to be less than 0.8 m. This slope was used as the longitudinal slope of the river tributaries. Similarly, the longitudinal slope of the river bed was approximated by the SRTM data.

Frequency analysis of historical daily discharge dataset at Tezpur gauging station (from 1983 until 2004) was carried out to compute the flood waves for various return periods (2, 5, 10, 15, and 20 years). A typical stage hydrograph of a river with large catchment size during a monsoon period (rainy season) is depicted in Figure 7. During the monsoon period, a number of flood waves can be noticed in the hydrograph, which are mainly due either to many clustered storm events or antecedent wet conditions. Among them, a few flood waves with distinct characteristics were identified (see Figure 8).

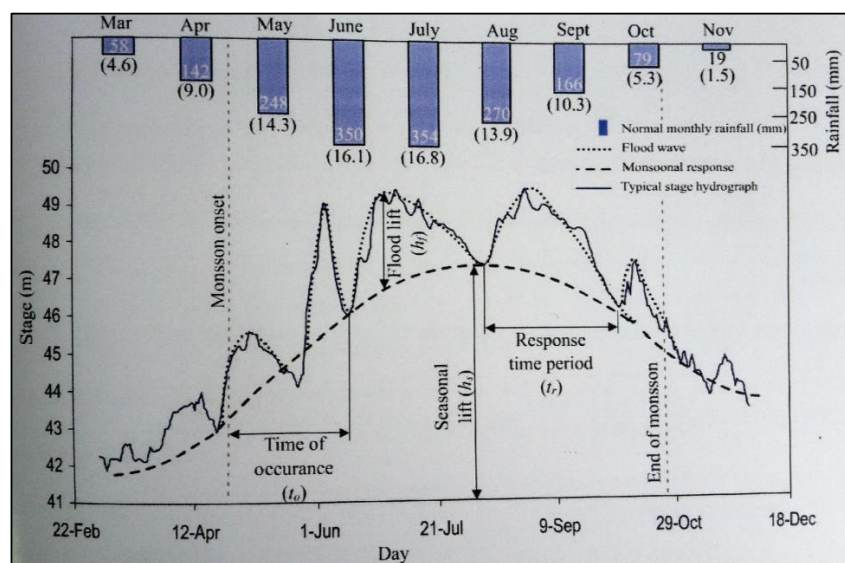


**Figure 8.** Schematic diagram for approximating stage hydrograph for a river basin. Normal monthly rainfall depth is superimposed on the diagram (the number within the brackets indicates the mean number of monthly rainy days).

The obtained hydrograph characteristics were found to be similar over the years and could be separated into two components, namely flood wave and monsoonal response. The flood waves are the fast response due to the occurrence of a severe and clustered storm event in the river basin. The other component was the average response of monsoonal rainfall. As the monsoon progresses, part of the river basin becomes saturated and its runoff response then becomes greater [34]. This helped in identifying the duration of individual flood events. The monsoonal response was approximated using Maxwell distribution [35]. The distribution suggested by Maxwell (1960) gives a better approximation

of the flood wave as it considers the correlations of peak flows with length ratios [36]. The generalized Maxwell distribution function used for this approximation is given by the following expression:

$$h(t) = h_b + h_s \left[ \frac{t}{k_s} \exp \left( 1 - \frac{t}{k_s} \right) \right]^{r_s}, \tag{3}$$

where  $h_b$  is the initial stage,  $h_s$  is the seasonal lift of monsoonal response,  $t$  is the base time, and  $k_s$  and  $r_s$  are the fitting parameters depending on the time to peak and base period of the seasonal response, respectively.

For a single flood wave, we can approximate characteristics using Maxwell distribution:

$$h^i(t) = h_f^i \left[ \frac{t}{k_f^i} \exp \left( 1 - \frac{t}{k_f^i} \right) \right]^{r_f^i} \text{ when } t_0^i \leq t \leq (t_0^i + t_r), \tag{4}$$

where,  $h^i(t)$  is the height of the lift of the  $i$ th flood wave at time  $t$ ,  $h_f^i$  is the maximum lift of the  $i$ th flood wave,  $k_f^i$  and  $r_f^i$  are the fitting parameters,  $t_0^i$  is the time of occurrence, and  $t_r$  is the response time period. For  $n$  number of flood waves, and superimposing them on the monsoonal response, we get:

$$h(t) = h_b + h_s \left[ \frac{t}{k_s} \exp \left( 1 - \frac{t}{k_s} \right) \right]^{r_s} + \sum_{i=1}^n h_f^i \left[ \frac{t}{k_f^i} \exp \left( 1 - \frac{t}{k_f^i} \right) \right]^{r_f^i}. \tag{5}$$

The lift of monsoonal response can be computed from its relation with total seasonal rainfall ( $R_s$ ) at the basin level. Then we can write

$$h_s = f_1(R_s). \tag{6}$$

Similarly, annual maximum flood lift,  $h_f^m$ , can be computed using frequency analysis. For a given return period ( $T$ ), it becomes:

$$h_f^m = f_2(T). \tag{7}$$

For simplification, the fitting parameters,  $k_f^i$  and  $r_f^i$  can be substituted with the most frequently occurring values,  $k_f$  and  $r_f$ . Finally, after substitution, the equation can be written as:

$$h(t) = h_b + f_1(R_s) \left[ \frac{t}{k_s} \exp \left( 1 - \frac{t}{k_s} \right) \right]^{r_s} + f_2(R_s) \left[ \frac{t}{k_f} \exp \left( 1 - \frac{t}{k_f} \right) \right]^{r_f} + \sum_{i=1}^{n-1} h_f^i \left[ \frac{t}{k_f^i} \exp \left( 1 - \frac{t}{k_f^i} \right) \right]^{r_f^i}. \tag{8}$$

Details of the different parameters used in the above equation are presented in Table 1.

**Table 1.** Details of different parameters with a brief description.

Variables	Computation Procedure
Initial stage	Determined from mean minimum stage just before monsoon onset
Season lift	Determined from the relationship of total monsoonal rainfall over entire basin
Fitting parameters	Used median value from historical data
Time period for monsoonal lift	Considered the total period of monsoon
Annual max. flood lift	Computed using frequency analysis for a given return period
Subsequent lifts of flood wave	Generated based on their distribution function
Time of occurrence of flood	Generated based on their distribution function

Two random variables listed in Table 2 were computed by random number generation techniques, which require the mean and standard deviation of a random variable and its best probability distribution. Random number generation for different probability distribution is carried out as described by [37]. The required parameters in the random number generation technique were computed from the characteristics of flood waves in the historical stage records. For the purpose, individual flood waves were fitted with the Maxwell distribution function by minimizing the

summation of absolute error using the Microsoft Excel optimization routine, which follows a generalized reduced gradient method.

**Table 2.** Probable lift of flood wave.

Return Period (Years)	Gauging Stations (in m)	
	Guwahati	Tezpur
2	2.39	2.28
5	2.87	2.8
10	3.11	3.07
15	3.24	3.2
20	3.32	3.29
30	3.42	3.4
50	3.54	3.53
100	3.68	3.68

It was observed that the lift of monsoonal response for the Maxwell function mainly depends on the total monsoonal rainfall. Results indicated a logarithmic relationship ( $r^2 = 0.84$ ) between monsoonal lift and total rainfall (Figure 9).

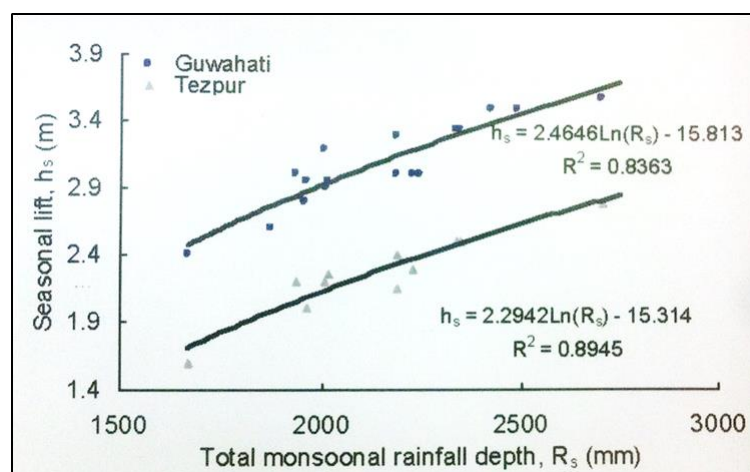


**Figure 9.** Relationship between the total monsoonal rainfall and monsoonal lift for the gauging stations considered in the study area.

In the model setup, upstream discharge hydrograph needs to be given as input data. In the previous section, probable stage variation at Tezpur gauging station was estimated using historical gauge records (from 1983 to 2004). Since the nodal is located at the upstream of Tezpur, the trend of the stage has been assumed to be the same as for the Tezpur gauging station. With known flow depth and Manning roughness coefficient, the average velocity at the nodal was computed. Using the velocity and flow area, the discharges were computed for different flood wave return periods and monsoon conditions as per Manning's resistance equation:

$$V = \frac{k}{n} R_h^{\frac{2}{3}} \cdot S^{\frac{1}{2}}, \quad (9)$$

where  $V$  is the cross-sectional average velocity (m/s);  $k$  is a conversion constant equal 1.0 for SI units;  $n$  is the Gauckler–Manning coefficient (independent of units);  $R_h$  is the hydraulic radius (m); and  $S$  is the slope of the water surface or the linear hydraulic head loss.

Using the velocity and flow area, the discharges were computed for different flood wave return periods and monsoon conditions (Table 3).

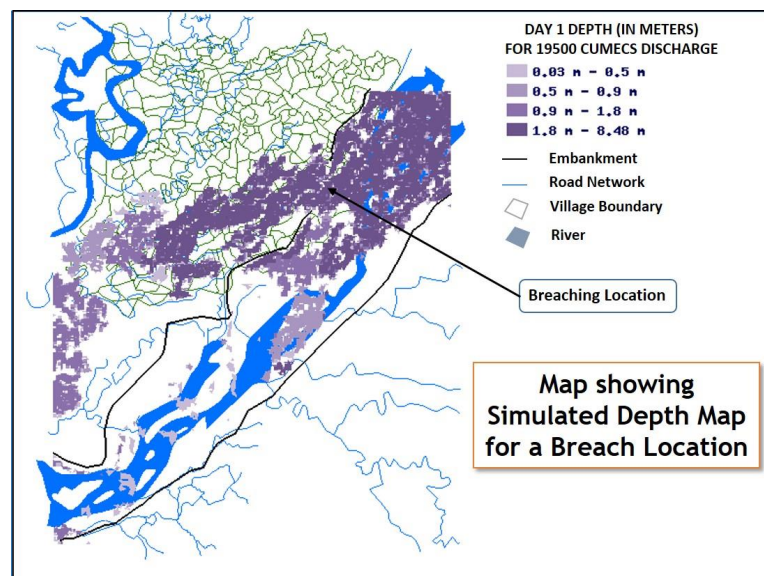
**Table 3.** Variation of discharge at the upstream nodal with monsoon condition and flow wave of different return periods [26].

Sr. No.	Return Period (years)	Monsoon Conditions	Discharge (m <sup>3</sup> /s)
1	2	Dry	13,082.8
2	5	Dry	15,902.3
3	10	Dry	17,451.30
4	15	Dry	18,217.38
5	20	Dry	18,732.83
6	2	Normal	16,197.25
7	5	Normal	19,252.09
8	10	Normal	20,919.88
9	15	Normal	21,742.39
10	20	Normal	22,319.17
11	2	Wet	19,464.99
12	5	Wet	22,739.25
13	10	Wet	24,517.54
14	15	Wet	25,393.44
15	20	Wet	26,006.55

Note: Monsoon conditions: A monsoon may be associated with dry weather as well as wet weather. A “wet” monsoon phase includes warm, moist air and a “dry” monsoon consists of cool, dry air. A normal monsoon is when the total amount of rainfall in the country between June and September is within 10 per cent (plus or minus) of the average rain over a long period.

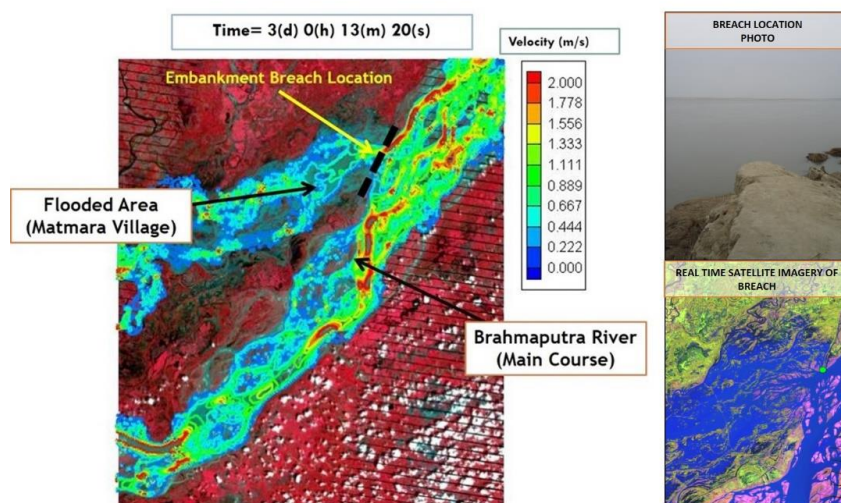
Stage variation at the downstream nodal was also defined in the model setup to define the boundary conditions downstream. For this purpose, stage gauge records of the Brahmaputra River, which is also the confluence of lower Subansiri River, were analyzed for the years 2001, 2003, and 2004. The highest flood level was found to be 81 m above mean sea level (i.e., the maximum water level at the river confluence is 81 m above mean sea level). The maximum gauge height at the downstream nodal was calculated with the Highest Flood Level (HFL) and average bed slope between the nodal and the gauging station. The calculated maximum water surface level at the nodal was 86 m asl.

The CCHE2D hydrodynamic model was then set up for the Subansiri flood plain, which was 14 km upstream of the breaching point. The computational mesh was also constructed using SRTM topographic data. The CCHE2D hydrodynamic model has one calibration parameter, i.e., bed roughness formula. Trial runs of the model wave were carried out for evaluating this parameter. In order to evaluate the performance in flood inundation prediction, satellite imagery for the same period (September 2008), when the actual breach happened, was used and verified the flooding around the embankment breaching location. Results show that the simulated flood inundation area for 26,000 m<sup>3</sup>/s discharge matched the flood-inundated area obtained from the abovementioned satellite imagery with 85% accuracy. Variation of flood inundation from the same breach location under different inflow (discharge) conditions was also estimated. Later the model was run to calculate steady discharge for a time period of three days and a flood hazard map was prepared by spatially analyzing the simulated inundation depth and the maximum scalar velocity, based on the depth–velocity hazard curves (Figure 10a,b). The curves are given by ACER Technical Memorandum No. 11 (1988) [38].



(a)

Model Output showing an Embankment Breach Scenario at Matmara village in Assam



(b)

**Figure 10.** (a) Map showing simulated depth map for a breach location (Day 1 depth (in meters) for 19,500-cumec discharge. (b) Map showing simulated velocity map for a breach location (Day 3 (in m/s) for 19,500-cumec discharge.

## 6. Conclusions

With a proliferation of free earth observation data and an abundance of free and open-source GIS software (PostgreSQL—PostgreSQL Global Development Group; UMN MapServer—MapServer Project Steering Committee (PSC); ka-Map—Ominiverdi; PostgreSQL, PostGIS—Refractions Research, British Columbia, Canada; Apache Web Server—The Apache Software Foundation, Massachusetts, USA; Windows Server 2003—Microsoft, Washington, US) and hydrodynamic models, flood monitoring has garnered more research and the resultant solutions are seen to be more efficient. However, with India's varied topography, a humongous network of rivers and streams, a unique population problem, and a ubiquitous data crunch, there is an obvious need for remote sensing in managing and monitoring disasters like floods. The semi-automatic method adopted in delineating water features

from microwave data is efficient, rapid, and accurate enough for mapping large areas. The logarithmic transformation helps to accurately classify water pixels from microwave data and reduces the dynamic range of the image, enabling faster processing. It is essential for near real-time systems. The algorithm was implemented using Java and the run time was approximately 8 min, making the proposed method useful for near real-time applications. The results obtained from the hydrodynamic investigation, carried out to simulate the flood behavior and the flood propagation in the low-lying flood plain area, provided information regarding the inundation depth within the flood plain and their spatial variation. The probabilistic flood hazard maps were generated and the highly vulnerable flood inundation zone in the flood plain was identified. This information can be used to plan appropriate cost-effective flood mitigation schemes at both pre- and post-breach scenarios. The result was compared with another source of data (official government figures) and the accuracy was in the range of 80–85%.

Identification of the potentially vulnerable sites for embankment breaching was also carried out but, due to an absence of information regarding the material used and type of construction of embankment, could not be completed. In addition, the prediction of levee-breaching conditions (local and extent) required more local geotechnical conditions and river hydraulics, which were not within the current scope of the project. In future studies, potential breach point identification would be studied so that the exact location of a breach can be provided to the district administration well in advance.

FRS was an attempt to provide a spatial component along with the assessment and querying capability to the user for a more comprehensive real-time understanding of the situation. FRS uses the inherent capabilities of a 'Geographical Information System' (GIS), which not only provides better visualization in the form of maps but also has analytic capabilities as an added advantage over traditional maps. This facilitates decision-making to a great extent. The traditional flood response system of the district administration involves relying on reports, mainly in the form of hard copies, and sometimes encounters unavailability of the same until it is too late. The query modules provided in FRS, along with the maps, help the authorities to correctly analyze the situation in much less time and much more accurately, as this process is devoid of the human interference factor. This is one of the most unique features of the system. Efficient use of this dataset through GIS and information technology is extremely helpful in deriving meaningful information necessary for better post-disaster operations. Modules like querying damage assessment and boat level information are unique and have been put together for the first time, to the knowledge of the authors, in a web-based platform.

**Special Note:** Right from the inception to completion of the project, there was continuous involvement from the stakeholders. Two stakeholder meetings, one training workshop, and numerous discussions were organized with the State and District Disaster Management Authorities and the Deputy Commissioner of North Lakhimpur so as to take their feedback/suggestions. Over 60 people from the various state departments and BDOs under the Lakhimpur District Administration were trained on Remote Sensing and GIS through lectures and demonstrations to help them understand how to effectively optimize the usage of FRS. Apart from training, all the relevant feedback was incorporated in developing the functionalities of the FRS. The Deputy Commissioner (DC), North Lakhimpur considered the system "promising" and ordered immediate usage of the system during flood seasons. The features included in the system were appreciated for their usability and practicality and were cited to be of utmost help to the DC office and allied departments dealing with floods. The local authorities, viz. ASDMA vouched for the usability of such a system and believed that such scientific verification would help them negate the human errors present in the current system. The FRS was also highly appreciated by the National Disaster Management Authority, Govt. of India in a national workshop held in Delhi in 2010. Apart from excellent reviews from peer groups and users, the Flood Response System has received many awards at the national level for innovative use of geospatial technology for disaster management. FRS received the India Geospatial Excellence Award for the year 2012, was recognized as a Finalist by the Grand Jury of eNortheast Award and received the Certificate of Recognition for the year 2012, was given an SKOCH Order of Merit in 2013, and in 2015 FRS was given a certificate of appreciation from eAssam Award, again in the innovative category.

**Acknowledgments:** The Flood Response System is the result of the Ministry of Information Technology's (MIT) initiation and C-DAC's effort towards research-oriented development activities with a special emphasis on the northeastern region of India. We are thankful to MIT, the Govt. of India for providing such an opportunity to work and deliver a solution in the form of a Flood Response System. We would also like to thank the CCHE2D developer team, Univ. of Mississippi (USA) for providing this robust hydrodynamic software for free.

**Author Contributions:** Yogesh Singh conceived and designed the Flood Response System; undertook field studies to collect real time data for embankment breaching; performed the microwave analyses; contributed in paper

writing; Upasana Dutta conceived and designed the Flood Response System; undertook field studies to collect real time data for embankment breaching; created and analysed the spatial and aspatial database; contributed in paper writing; T.S. Murugesh Prabhu performed the microwave analyses; contributed in paper writing; I. Prabu developed the Flood Response System; contributed in paper writing; Jitendra Mhatre developed the Flood Response System; Sandeep Srivastava was the mentor and contributed in data and analysis; contributed in paper writing; Manoj Khare contributed in project coordination and analysis of data; Subasisha Dutta performed the Probabilistic Inundation analyses.

**Conflicts of Interest:** The authors declare no conflict of interest.

## References

1. DFO. Global Active Archive of Large Flood Events, 2009. Available online: [http://www.dartmouth.edu/\\*floods](http://www.dartmouth.edu/*floods) (accessed on 25 February 2009).
2. FTS OCHA. Financial Tracking Service, 2009. Available online: <http://ocha.unog.ch/fts> (accessed on 25 February 2009).
3. Rodriguez, J.; Vos, F.; Below, R.; Guha-Sapir, D. *Annual Disaster Statistical Review 2008*; Centre for Research on the Epidemiology of Disasters: Brussels, Belgium, 2009.
4. The United Nations Office for Disaster Risk Reduction (UNISDR). The Human Cost of Weather Related Studies. 2015. Available online: [https://www.unisdr.org/2015/docs/climatechange/COP21\\_WeatherDisastersReport\\_2015\\_FINAL.pdf](https://www.unisdr.org/2015/docs/climatechange/COP21_WeatherDisastersReport_2015_FINAL.pdf) (accessed on 12 December 2016).
5. Flood List, 2016. UN–1995 to 2015, Flood Disasters Affected 2.3 Billion and Killed 157,000, 2016. Available online: <http://floodlist.com/dealing-with-floods/flood-disasterfigures-1995-2015> (accessed on 25 February 2009).
6. Waghmare, M.S.; Hire, R.; Hailkar, S. A Review on Evaluation and Development of Effective Flood Forecasting, Warning and response System. *IOSR J. Mech. Civ. Eng.* **2015**, 137–141.
7. Shiva, S.V.; Sharma, P.; Srinivasa, R.G.; Bhanumurthy, V. Development of village-wise flood risk index map using multi-temporal satellite data: A study of Nagaon district, Assam, India. *Curr. Sci.* **2012**, 103, 25.
8. De Groeve, T. Flood monitoring and mapping using passive microwave remote sensing in Namibia. *Geomat. Nat. Hazards Risk* **2010**, 1, 19–35. [[CrossRef](#)]
9. Jensen, J.R. *Remote Sensing of the Environment: An Earth Resource Perspective*; Prentice-Hall: Upper Saddle River, NJ, USA, 2007; p. 592.
10. Klemas, V. Airborne remote sensing of coastal features and processes: An overview. *J. Coast. Res.* **2013**, 29, 239–255. [[CrossRef](#)]
11. Puech, C.; Raclot, D. Using geographical information systems and aerial photographs to determine water levels during floods. *Hydrol. Process.* **2002**, 16, 1593–1602. [[CrossRef](#)]
12. Webster, T.L.; Forbes, D.L.; Dickie, S.; Shreenan, R. Using topographic lidar to map flood risk from storm-surge events for Charlottetown, Prince Edward Island, Canada. *Can. J. Remote Sens.* **2004**, 30, 64–76. [[CrossRef](#)]
13. Brivio, P.A.; Colombo, R.; Maggi, R.; Tomasoni, R. Integration of remote sensing data and GIS for accurate mapping of flooded areas. *Int. J. Remote Sens.* **2002**, 23, 429–441. [[CrossRef](#)]
14. Reid, S.K.; Tissot, P.E.; Williams, D.D. Methodology for applying GIS to evaluate hydrologic model performance in predicting coastal inundation. *J. Coast. Res.* **2014**, 30, 1055–1065. [[CrossRef](#)]
15. Smith, L.C. Satellite remote sensing of river inundation area, stage and discharge: A review. *Hydrolog. Process.* **1997**, 11, 1427–1439. [[CrossRef](#)]
16. Horritt, M.S.; Mason, D.C.; Luckman, A.J. Flood boundary delineation from Synthetic Aperture Radar imagery using a statistical active contour model. *Int. J. Remote Sens.* **2001**, 22, 2489–2507. [[CrossRef](#)]
17. Lawrence, M.K.; Walker, N.D.; Balasubramanian, S.; Baras, J. Application of Radarsat-1 synthetic aperture radar imagery to assess hurricane-related flooding of coastal Louisiana. *Int. J. Remote Sens.* **2005**, 26, 5359–5380.
18. Townsend, P.A.; Walsh, S.J. Modeling floodplain inundation using an integrated GIS with radar and optical remote sensing. *Geomorphology* **1998**, 21, 295–312. [[CrossRef](#)]
19. Stevens, T.B. Synthetic Aperture Radar for Coastal Flood Mapping, NASA Global Change Master Directory, Data Originator. LSU Earth Scan Laboratory: Baton Rouge, LA, USA, 2013. Available online: <http://www.esl.lsu.edu/home/> (accessed on 6 November 2016).

20. Bjerklie, D.M.; Dingman, S.L.; Vorosmarty, C.J.; Bolster, C.H.; Congalton, R.G. Evaluating the potential for measuring river discharge from space. *J. Hydrol.* **2003**, *278*, 7–38. [[CrossRef](#)]
21. Klemas, V. Remote Sensing of Floods and Flood-Prone Areas: An Overview. *J. Coast. Res.* **2014**, *31*, 1005–1013. [[CrossRef](#)]
22. Singh, Y.; Ferrazzoli, P.; Rahmoune, R. Flood monitoring using microwave passive remote sensing (AMSR-E) in part of the Brahmaputra basin, India. *Int. J. Remote Sens.* **2013**, *34*, 4967–4985. [[CrossRef](#)]
23. Baldassarre, G.D.; Castellarin, A.; Montanari, A.; Brath, A. Probability-Weighted Hazard Maps for Comparing different Flood Risk Management Strategies: A Case Study. *Nat. Hazards* **2009**, *50*, 479–496. [[CrossRef](#)]
24. Barbetta, S.; Camici, S.; Bertuccioli, P.; Palladino, M.R.; Moramarco, T. Levee Body Seepage: A Refinement of an Expedient Procedure for Fragility Curves and Vulnerability Diagrams' Assessment. *Hydrol. Res.* **2017**. [[CrossRef](#)]
25. Mazzoleni, M.; Bacchi, B.; Barontini, S.; di Baldassarre, G.; Pilotti, M.; Ranzi, R. Flooding Hazard Mapping in Floodplain Areas Affected by Piping Breaches in the Po River, Italy. *J. Hydrol. Eng. ASCE* **2014**, *19*, 717–731. [[CrossRef](#)]
26. Dutta, S.; Medhi, H.; Karmaker, T.; Singh, Y.; Prabu, I.; Dutta, U. Probabilistic Flood Hazard Mapping For Embankment Breaching. *ISH J. Hydraul. Eng.* **2010**, *16*, 15–25. [[CrossRef](#)]
27. Karmaker, T.; Dutta, S.; Fisher, M. Modelling Large Scale Flood Inundation for Risk Assessment. In Proceedings of the SPIE Asia-Pacific Remote Sensing Conference, Goa, India, 13–17 November 2006.
28. National Center for Computational Hydroscience and Engineering, CCHE2D ver 3.0. Available online: [https://www.ncche.olemiss.edu/sites/default/files/files/docs/1d\\_applications.pdf](https://www.ncche.olemiss.edu/sites/default/files/files/docs/1d_applications.pdf) (accessed on 25 February 2009).
29. Goswami, D.C. Fluvial regime and Flood Hydrology of the Brahmaputra River Assam. In *Flood Studies in India*; Kale, V.S., Ed.; Geological Society of India: Bengaluru, India, 1998; Volume 41, pp. 53–75.
30. Maidment, D.R.; Evans, H.R. Community Flood Response System, 2015. Available online: <http://www.ce.utexas.edu/prof/maidment/NFIE/Docs/CommunityFloodResponseSystem.pdf> (accessed on 25 February 2015).
31. WRIS, India. Available online: <http://www.india-wris.nrsc.gov.in/wrpinfo/index.php?title=Brahmaputra> (accessed on 25 February 2009).
32. WAPCOS. *Morphological Studies of River Brahmaputra*; WAPCOS: Water and Power Consultancy Services (India) Limited: New Delhi, India, 1993.
33. Gonzalez, R.C.; Woods, R.E. *Digital Image Processing*; Pearson Education: Delhi, India, 2006; ISBN 9332570329.
34. Chattopadhyay, A.; Dutta, S. Mapping monsoonal soil wetness regions using multi-temporal vegetation dataset. *Int. J. Remote Sens.* **2006**, *27*, 4693–4700. [[CrossRef](#)]
35. Spiegel, M.R. *Schaum's Outline of Theory and Problems of Probability and Statistics*; McGraw-Hill: New York, NY, USA, 1992; p. 119.
36. Howard, A.D. Theoretical Model of Optimal Drainage Networks. *Water Resour. Res.* **1990**, *26*, 2107–2117. [[CrossRef](#)]
37. Wang, W. A Hydrograph-Based Prediction of Meander Migration. Ph.D. Thesis, Texas A & M University, College Station, TX, USA, 2006.
38. ACER Technical Memorandum NO. 11. In *Downstream Hazard Classification Guidelines*; Assistant Commissioner-Engineering and Research, Bureau of Reclamation, United States Department of the Interior: Denver, CO, USA, 1988.

